Comparison of persistence in spot versus flat field illumination and single pixel response on a Euclid HAWAII-2RG at ESTEC

Pierre-Elie Crouzet, Ludovic Duvet, Paolo Strada, Ralf Kohley, Remi Barbier, et al.

Pierre-Elie Crouzet, Ludovic Duvet, Paolo Strada, Ralf Kohley, Remi Barbier, Thierry Beaufort, Sander Blommaert, Bart Butler, Gertjan Van Duinkerken, David Gooding, Joerg Ter Haar, Jerko Heijnen, Frederic Lemmel, Cornelis Van der Luijt, Hans Smit, Visser Ivo, "Comparison of persistence in spot versus flat field illumination and single pixel response on a Euclid HAWAII-2RG at ESTEC," Proc. SPIE 9915, High Energy, Optical, and Infrared Detectors for Astronomy VII, 99151E (5 August 2016); doi: 10.1117/12.2230836

Event: SPIE Astronomical Telescopes + Instrumentation, 2016, Edinburgh, United Kingdom

Comparison of persistence in spot versus flat field illumination and single pixel response on a Euclid HAWAII-2RG at ESTEC

Pierre-Elie Crouzet[a], Ludovic Duvet[a], Paolo Strada[b] , Ralf Kohley[c], Rémi Barbier[d], Thierry Beaufort[a], Sander Blommaert[a] , Bart Butler[a] , Gertjan Van Duinkerken[a] , David Gooding[a], Joerg ter Haar[a] , Jerko Heijnen[a], Frederic Lemmel[a], Cornelis van der Luijt[a], Hans Smit[a] ,Ivo Visser[a]

[a] Future Missions Preparation Office, Payload Technology Validation Section
European Space Agency, ESTEC, Keplerlaan 1, 2200 Noordwijk, NL
[b] European Space Agency, ESTEC, Keplerlaan 1, 2200 Noordwijk, NL
[c] European Space Agency, ESAC, Camino Bajo del Castillo, s/n., Urb. Villafranca del Castillo, 28692 Villanueva de la Cañada, Madrid, Spain
[d] Institut de Physique Nucleaire de Lyon, 4, Bâtiment Paul Dira, Rue Enrico Fermi, 69622 Villeurbanne, France

ABSTRACT

Euclid is an ESA mission to map the geometry of the dark Universe with a planned launch date in 2020. Euclid is optimised for two primary cosmological probes, weak gravitational lensing and galaxy clustering. They are implemented through two science instruments on-board Euclid, a visible imager (VIS) and a near-infrared spectro-photometer (NISP), which are being developed and built by the Euclid Consortium instrument development teams. The NISP instrument contains a large focal plane assembly of 16 Teledyne HgCdTe HAWAII-2RG detectors with 2.3µm cut-off wavelength and SIDECAR readout electronics.

While most Euclid NISP detector system on-ground tests involve flat-field illumination, some performance tests require point-like sources to be projected onto the detector. For this purpose a dedicated test bench has been developed by ESA at ESTEC including a spot projector capable of generating a Euclid-like PSF. This paper describes the test setup and results from two characterisation tests involving the spot projector.

One performance parameter to be addressed by Euclid is image (charge) persistence resulting from previous exposures in the science acquisition sequence. To correlate results from standard on-ground persistence tests from flat-field illumination to realistic scenes, the persistence effect from spot illumination has been evaluated and compared to the flat-field.

Another important aspect is the photometric impact of intra-pixel response variations. Preliminary results of this measurement on a single pixel are presented.

Keywords: Euclid, HAWAII-2RG, persistence, photometric impact, ESA

1. INTRODUCTION

The combined focal plane for the Near-Infrared Spectrometer and Photometer (NISP) of the ESA medium class mission Euclid [1] comprises 16 custom-made HAWAII-2RG detector systems. Procurement of the flight detector systems is provided by NASA through JPL after a pre-development phase, which ESA started with Teledyne Imaging Sensors (TIS) in August 2012. One full pre-development detector system (detector, cryo-flex cable, readout electronics) has been integrated in a cryostat at ESTEC for two different test campaigns. The objective of the first test campaign was to perform a comparative analysis of the detector persistence behaviour under different illumination conditions, namely flat field versus spot illumination. The second test campaign had the goal of measuring the photometric impact of the detector intra-pixel variation using a Euclid representative spot illumination.

High Energy, Optical, and Infrared Detectors for Astronomy VII, edited by Andrew D. Holland, James Beletic,
Proc. of SPIE Vol. 9915, 99151E · © 2016 SPIE · CCC code: 0277-786X/16/$18 · doi: 10.1117/12.2230836

The first section of this paper describes the optical performances of the test set-up followed by sections on the comparison between persistence in flat field and spot illumination and the first results of a single pixel response to prepare the measurement of the photometric impact of intra-pixel variations.

2. TEST SET UP OPTICAL PERFORMANCES

The test bench developed at ESTEC allows different optical configurations on the detector under test. It allows to project a flat field with LEDs or a spot on the detector under test. The spot configuration is used for sub-pixel scanning and for persistence tests. All tests have been carried out in the Euclid operational thermal environment, which is 100K for the HAWAII-2RG and 145K for the SIDECAR readout electronics. The ground support equipment used to acquire and record the readout frames during the test execution, a Teledyne SAM card, was kept at room temperature.

2.1 Flat field illumination test set up

For the persistence test, a flat field illumination projected on the HAWAII-2RG detector with low background signal allows to measure persistence signal. An LED flange consisting of 5 LEDs and located on a 200K shield has been inserted into the cryostat (see Figure 1). The 5 LEDS, with a central wavelength of 1300nm are controlled in current and can be independently activated. To limit the background created by the 200K shield, a filter from Spectrogon has been inserted on a 90K filter wheel, in front of the cryostat. This filter has a half band width transmission of 70±10nm.

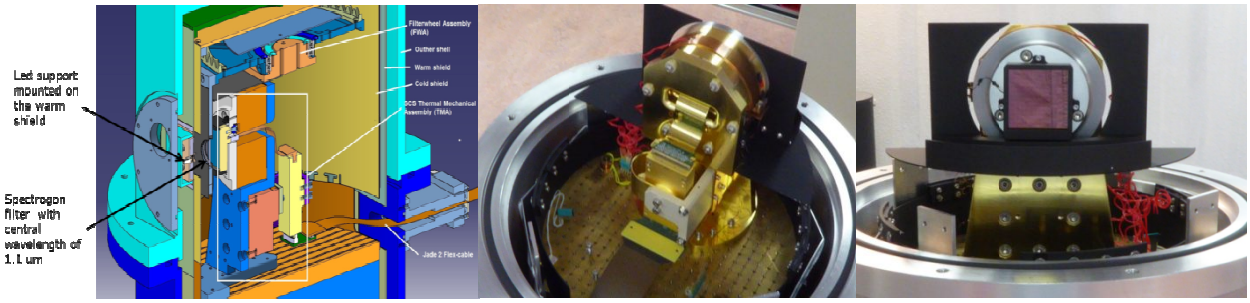

Figure 1 Left: Schematic view of cryostat with the LED support, the cold filter and the detector. Middle: back view of the detector with the readout electronic and flex cable. Right: Front view of the detector mounted in the cryostat

The 5 LEDs create a uniform illumination on the detector with a standard deviation around 3% of the mean value. The LED current can be adjusted to produce a flux between 10e/pxl/s and 3000e-/pxl/s.

Thanks to the narrow-band cold filter the level of background measured is around 0.1 e-/pxl/s. This level is low enough to probe the persistence behavior for our purpose.

2.2 Spot projector illumination test set up for sub-pixel scanning

To perform a sub-pixel scanning, a spot projector system designed at ESTEC and manufactured by Jenoptik Optical System (Germany) has been installed on the test bench.

This spot projector system contains of 6 lenses and has been originally designed to project a spot smaller than the pixel size for a measurement of intra-pixel variation on CCD detectors [2]. Figure 2 shows a drawing of the spot projector system with pinhole, the 6 lenses and the cryostat window (named “Wnd” on the drawing). The optics produce a magnification of ≈0.5.

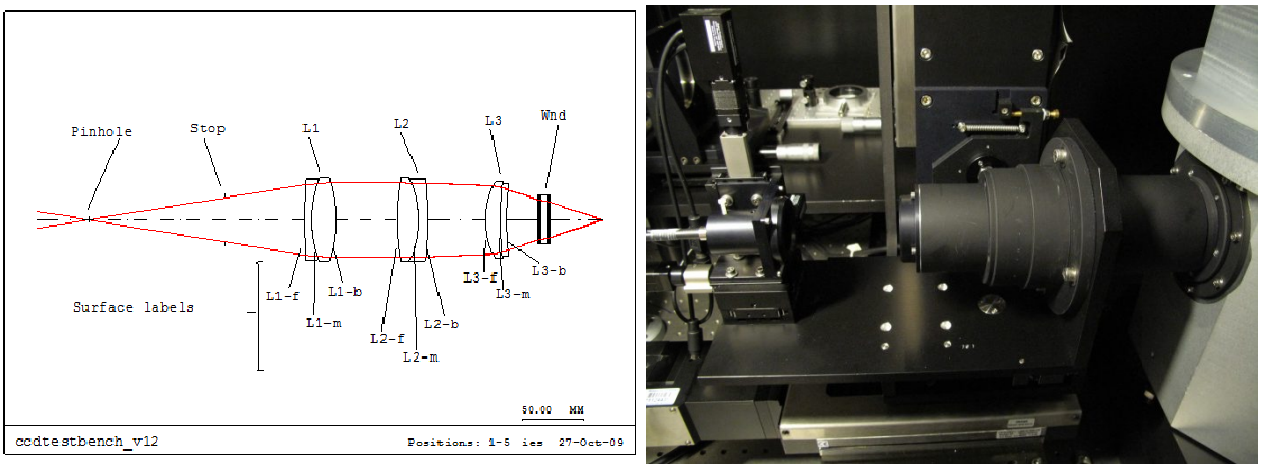

Figure 2 Left: Schematic view of the spot projector system. Right: Spot projector with the pinhole, lens system and the window of the cryostat.

A 25um diameter pinhole has been inserted in the spot projector to create a Euclid-like F#10 beam. The spot projector is mounted on a tip/tilt plate for alignment as well as on a separate micrometer-driven alignment stage for the pinhole.

The quality of the produced spot has been tested with a laser at 633nm and then with a 850nm LED on a dedicated and separate test bench.
This test bench (see Figure 3) comprises a light source, a 25um pinhole, the spot projector, an inverted microscope objective (magnification of factor 10) and a CCD camera. The CCD camera captures the Airy function in higher resolution to validate the quality of the produced beam in the infrared wavelength range.

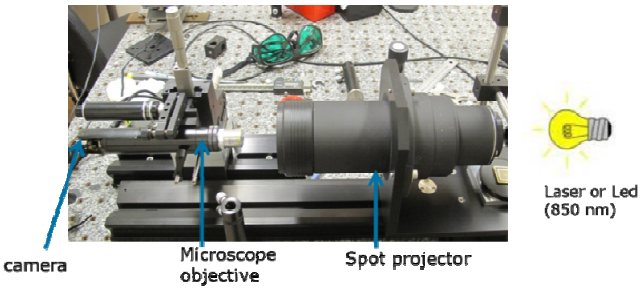

Figure 3: Photo of the test set-up with the spot projector, the microscope objective and the CCD camera.

Using the laser at 633nm wavelength, the diameter of the minima of the Airy function can be measured and compared to the theoretical value (see Figure 4). The deviations of measured to theoretical values between 0.5% and 4% indicate that the spot projector tested with the laser and a pinhole of 25um is producing the desire F#10 beam with adequate accuracy.

	Theory diameter of minima in pixel	Estimated diameter of minima in pixel number	Ratio to theory
First minima	25.7	27	1.04
Second minima	47.0	48	1.02
Third minima	68.3	68	0.99
4th minima (estimated on picture)	89.4	90	1.005
5th minima (estimated on picture)	110.5	112	1.012

Figure 4: Estimated Airy function minima and ratio to the expected theoretical values with a laser at 633nm.

Using an LED centered at 850nm with a bandwidth of 13nm, the associated Airy function is imaged as well. The estimated minima of the Airy function is measured again and compared to theory. The first minimum contains the highest measurement error (26%), since the spot needed to be highly saturated to be able to detect the following minima (see Figure 5).

	Theory diameter of minima in pixel	Estimated diameter of minima in pixel number	Ratio to theory
First minima	34.5	43	1.26
Second minima	63.2	64	1.01
Third minima	91.7	90	0.98

Figure 5: Estimated Airy function minima and ratio to the expected theory with an LED at 850nm.

Once the spot projector system was validated, it has been added to the Euclid detector test bench containing a 100W QTH lamp, a monochromator, an optical fiber to the spot projector, a sapphire window and the cryostat containing the HAWAII-2RG detector (see Figure 6).
To allow pixel scans with low background at three different infrared wavelengths, cold filters with central wavelengths of 1100nm, 1550nm and 1950nm were mounted on a filter wheel inside the cryostat.

The spot projector system is mounted on a 3 axis Newport precision motor translation stage allowing scan of a pixel in 2µm steps in the optical axis direction as well as in the plane perpendicular to the optical axis. An automatized data acquisition system developed in Python allows recording frames for each spot projector position and for each wavelength. The entire set up is mounted on a vibration controled optical table inside a dark enclosure.

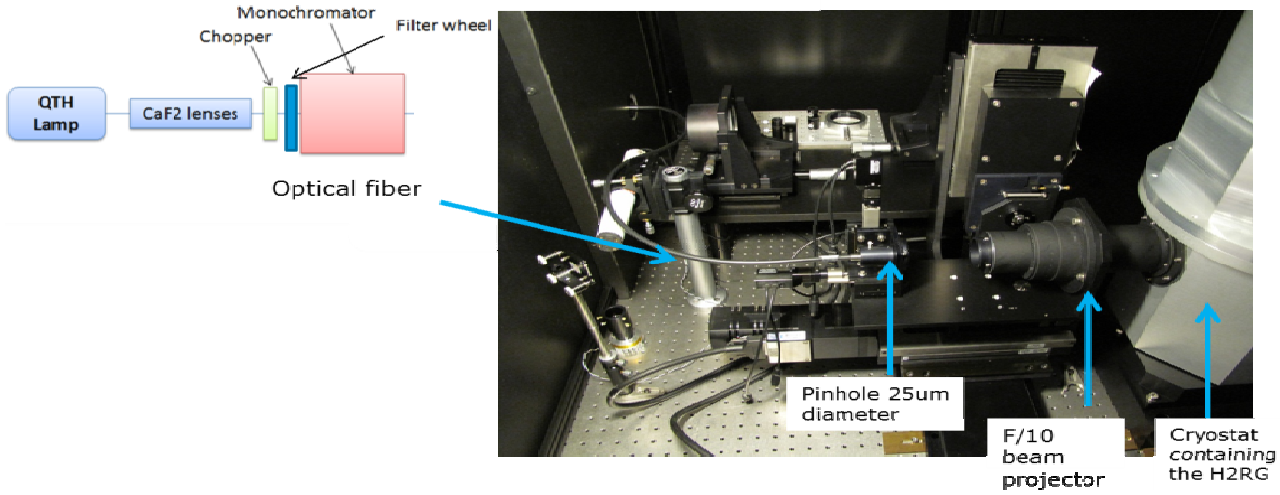

Figure 6: Drawing and picture of the test bench with the spot projector system mounted on 3 axis translation and the cryostat containing the HAWAII-2RG

2.3 Spot projector system for persistence test

To compare the persistence behavior caused by flat field and spot illumination, the spot projector system previously described can be de-focused to create a larger spot of a few pixels wide with a relatively flat top and sharp edges. This spot projector is then placed on the same test bench as used in the sub-pixel scanning configuration. Different illumination fluxes can be obtained by adjusting the slit size at the entrance of the monochromator. Figure 7 shows the flux received by the detector in the area of the flat top for different slit size.

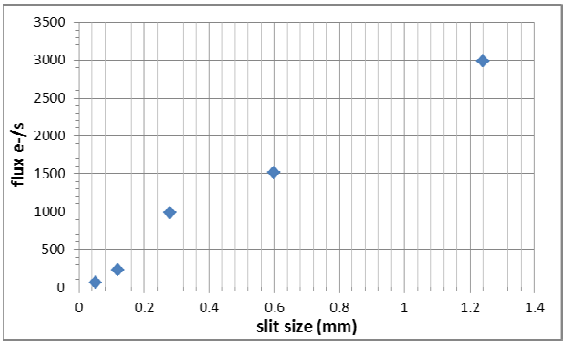

Figure 7: Flux received by the detector depending on the monochromator slit size

The defocused spot shape for a given slit size is shown in Figure 8. The width in the vertical and horizontal direction is around 7 pixels.

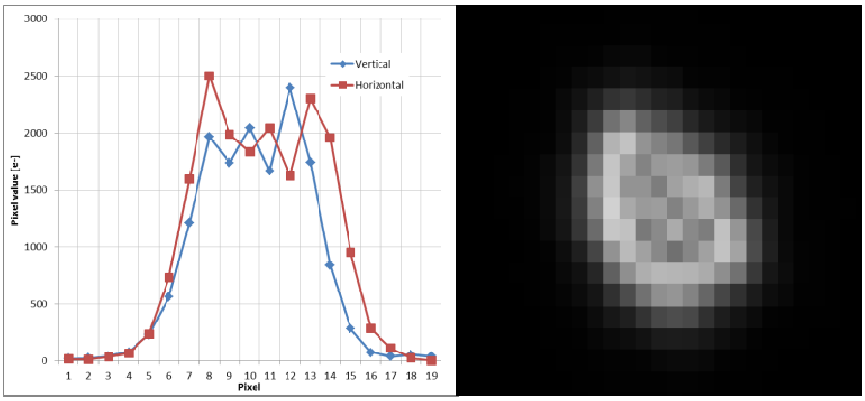

Figure 8: Left: Defocused spot vertical and horizontal cross section. Right: Associated spot recorded with the detector

To be able to measure a low level of persistence, a second filter centered on 1100nm wavelength was added inside the cryostat to decrease the black body radiation emitted by the test room. This filter, located on the 77K cryostat internal shield decreased the background to 0.1 e/pxl/s at detector level. This level of background, with a detector maintained at a temperature of 100K allows detecting the fast component of the persistence behavior.

3. FLAT FIELD VERSUS SPOT ILLUMINATION PERSISTENCE

The persistence behavior has been quantified as a first approximation with a linear least-square fit to the pixel values on the frames during the first 70s in the dark exposure following the 560s illumination used for the persistence stimulus. The goal of this study is to compare the persistence behavior in flat field versus spot illumination. This activity is complementary to the planned detector performance verification campaign, which relies on flat field illumination for full array statistics, to measure the persistence effect caused by point-like objects (stars and galaxies).

Still pending is the fitting of the persistence decay with multiple exponential functions instead of the linear fit approximation (see [3]), which is planned at a later stage.

3.1 Persistence in flat field illumination

The data were recorded using the test set up presented in section 2.1. For a given LED current, the data acquisition consists of 3 ramps of 450 up-the-ramp frames recorded with the LED switched off, followed by 15 groups of 17 reads and 14 drops frames (equivalent to the Euclid NISP 560 s integration time) with the LED switched on and then 1 ramp of 400 up-the-ramp frames recorded with LED off to measure the persistence level. A total of 7 different LED currents were set to create different illumination fluxes on the detector.

The dependence of persistence with the illumination level (see Figure 9) in the flat field configuration shows a linear dependency below full well (slope of 0.03 e/pxl/s/ke-), a sharp rise (transition zone) and then another linear dependency above full well. Each point of the plot represents one pixel of a 200x200 pixels window located in the middle of the array. The same window is used for the spot illumination persistence tests. The gradient of color represents the density of the pixels. The full well is estimated to be 110ke- given the applied reverse bias of 0.5V on the detector. The equivalent illumination is the extrapolated signal level on the detector after 560s of integration time, if the detector were not saturating before.

The persistence theory developed in [3] explains that traps located in the depletion zone around the bowl-shaped P-N junction are responsible for the persistence behavior with trapping at the moving depletion edge under charge accumulation. The depletion zone extends towards the surface close to the indium bumps. The number of surface traps is typically higher than the bulk traps as the surface is more sensible to crystal dislocation and impurities accounting for two different persistence regimes depending on which trapping mechanism prevails, with bulk trapping dominating for under full well fluences and surface trapping for over full well fluences. The linear dependency below full well seem to indicate a linear change in depletion volume with fluence.

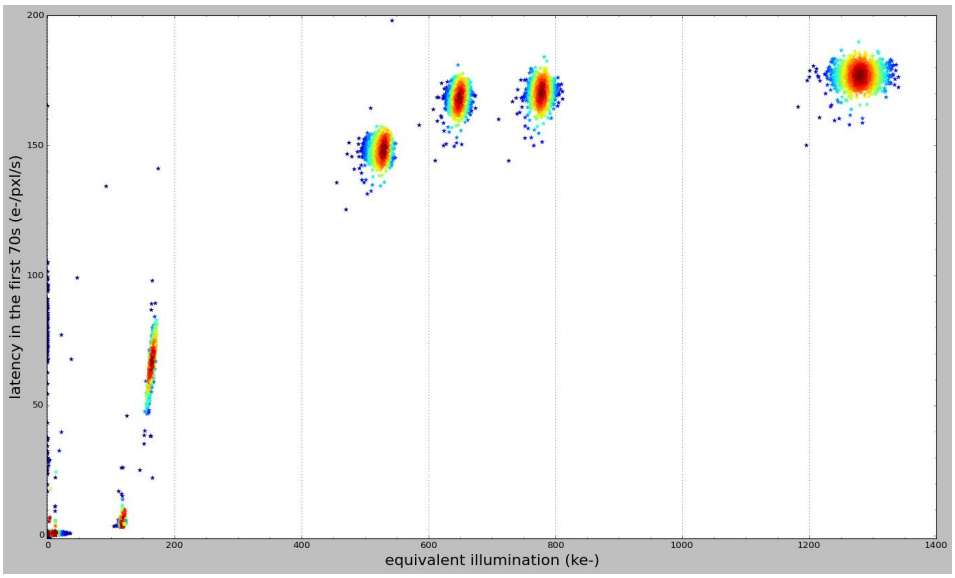

Figure 9: Dependence of persistence with equivalent illumination in the flat field configuration.

3.2 Persistence in spot illumination

With the data recorded with the spot illumination, the dependency of the persistence with the equivalent illumination can be plotted as well. In the following plots each marker represents the position of the pixels in the window with respect to the spot. The pixels located on top of the spot are marked as diamonds, the ones on the side of the spot as square and the ones out of the spot as circles. The spot profile traces different illumination levels for the same chosen illumination flux, from the top of the spot with the highest illumination to the area outside of the spot receiving no illumination. A total of 6 different illumination fluxes were chosen (see Figure 10).

In this figure one can notice that the transition zone shifts toward smaller equivalent illumination when the illumination flux as recorded on the top of the spot is higher. For the highest flux, the transition zone from low to high persistence starts already at around half full well and not as expected at full well. Similar results were observed on the Hubble WFC3 with stars of different intensity located in the field of view [5]. Nevertheless, this behavior is not expected.

For the lowest illumination flux (400 e/pxl/s) the persistence remains low even beyond full well fluences.

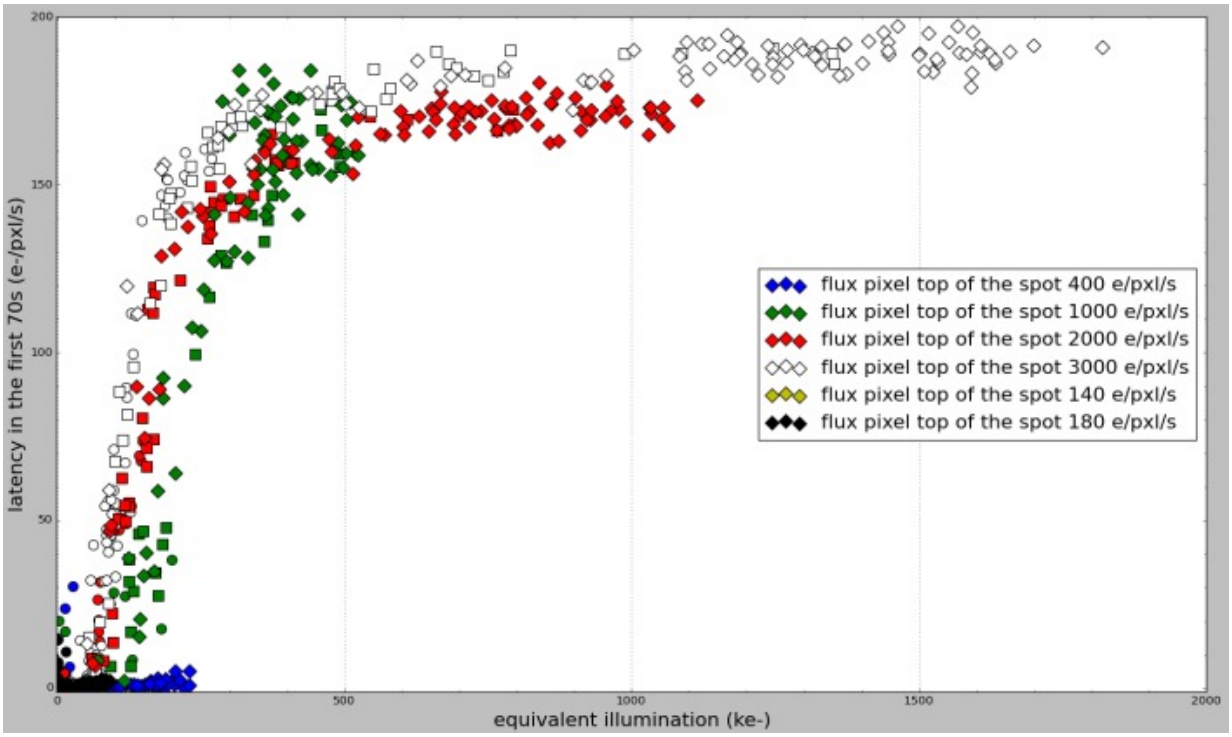

Figure 10: Evolution of the persistence in spot illumination for different incoming flux.

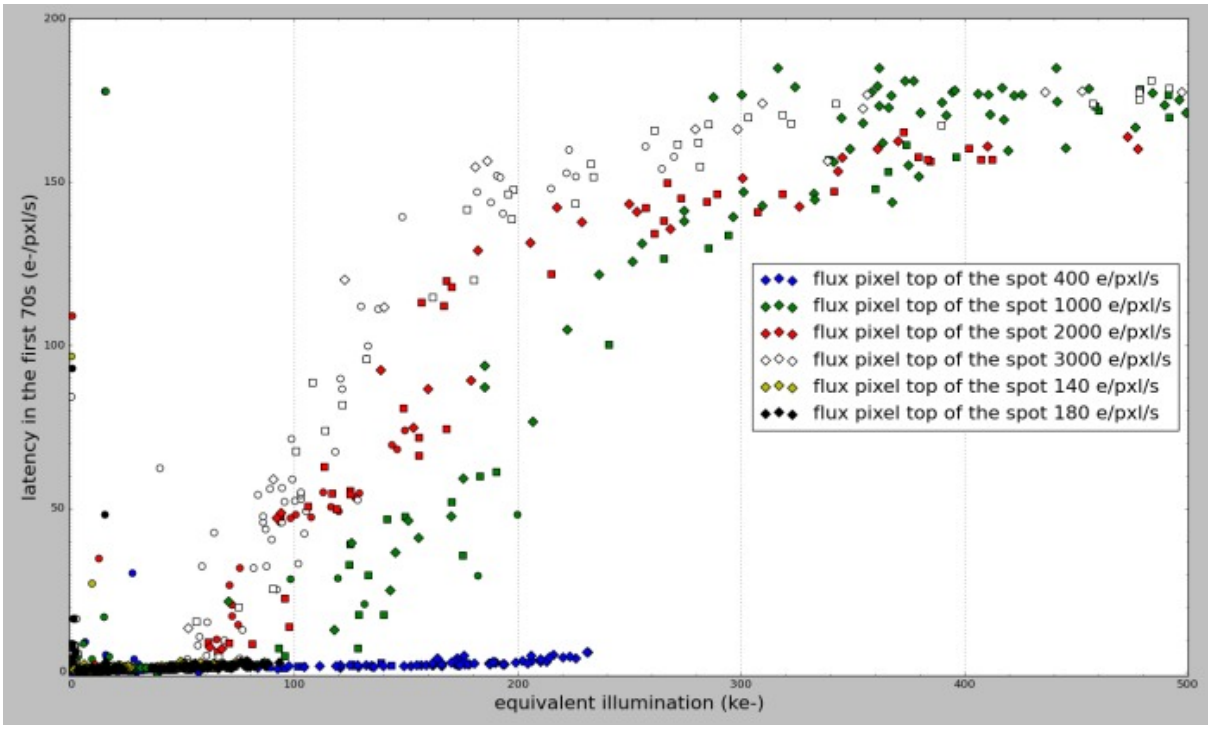

Figure 11: Same as Figure 10 but zoomed into the equivalent illumination range until 500ke-.

In order to find an explanation for the shift of the transition zone from low to high persistence, the evolution of the signal for adjacent pixels between the top of the spot and the side of the spot during the illumination ramp was plotted.

For the low flux illumination case (400 e-/pxl/s), the evolution of the signal with the integration time of pixels adjacent to saturated pixels is as expected (see Figure 12). Also saturated pixels exhibit a low latency indicating dominance of bulk trapping and not surface trapping. The resulting persistence is linear with the equivalent illumination and stay at a low level (below 10 e-/pxl/s). The surface traps seem to need a sufficient "soak time" to capture charges, which seems not accomplished in the low flux case.

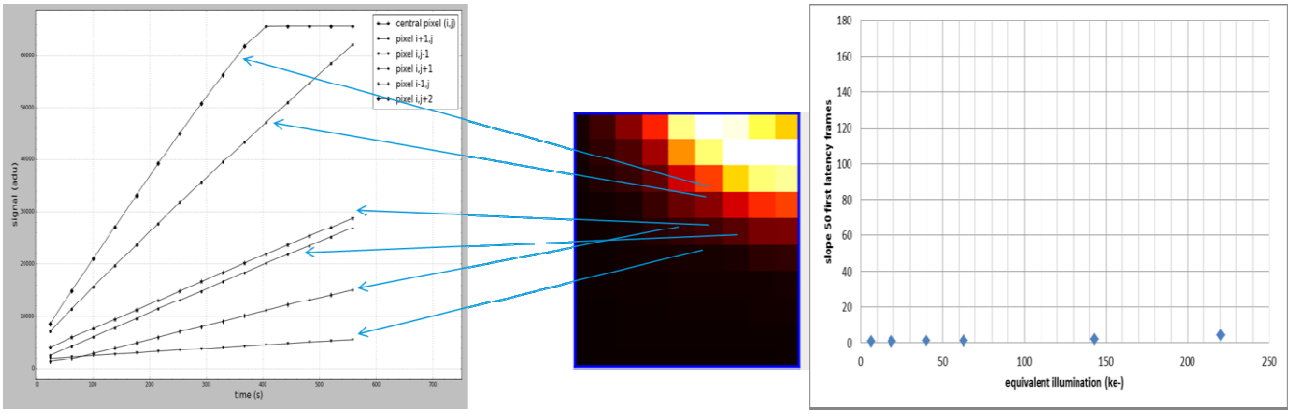

Figure 12 Left: Evolution of the signal for adjacent pixels with a low flux (180e-/pxl/s). Right: Persistence level for the same pixels. The persistence is linear even beyond full well

For the high flux illumination case, the saturated pixels influence the signal slope of the adjacent pixels that see an increase of signal not consistent with the level of light flux received (see Figure 13). This influence creates a high persistence behavior on the pixels, even if their fluence stays below saturation level. On Figure 13, once the pixel closest to the center of the spot is saturated for some time, the neighboring pixel sees an increase of flux not associated to the illumination. The total increase of signal due to the excess flux is around 4800 electrons. This increase of signal could be a non-linearity effect in the inter-pixel capacitance (IPC) and/or diffusion of charges between pixels.

If it were purely an IPC effect, the additional coupling between the adjacent pixels would be around 25%, far above the expected 0.6% measured at a lower flux on this detector. Additionally, others (see references [6] and [7]) report a constant IPC with signal measured on coupling around hot pixels. Even assuming a slight dependence of IPC with signal, the 25% of coupling would be difficult to explain.

Intra-pixel measurements ([8], [9]) on HAWAII-2RG detectors (respectively 1.7µm and 5µm cut off) indicate that the primary contributor to the pixel response profile shape is the diffusion in the bulk detector material. Ignoring any brighter-fatter effect, this diffusion is always present and linear with signal and therefore cannot be attributed to a sudden increase in signal in adjacent pixels. In our case, once a pixel reaches saturation of the infrared diode, the depletion zone collapses and charges from the saturated pixel seem to diffuse to the neighbor pixels along the surface with charge being captured by the surface traps, not only in the area associated to the saturated pixel but also in the adjacent one. These surface traps release then the charges as persistence during the dark exposure accounting for the higher than expected persistence signal.

The persistence behavior of a given pixel depends not only on the fluence it received but also on the amount of soaking time spent by its neighbor pixels in saturation.

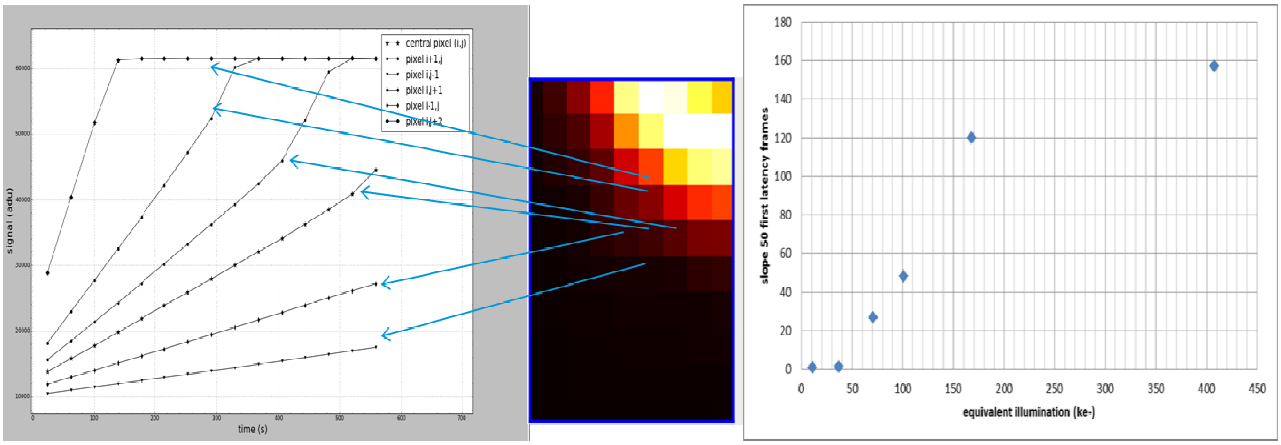

Figure 13: Left: Evolution of the signal for adjacent pixels with a high flux (2000e-/pxl/s). Right: Persistence level for the same pixels. The persistence rises sharply at about half of full well.

3.3 Flat field versus spot illumination persistence

The flat field and spot illumination persistence data can be now combined in a single plot (see Figure 14 and Figure 15). For the low flux (400 e-/pxl/s), the persistence in flat field and spot are equivalent. For higher fluxes, the soaking time in saturation of pixels located inside of the spot influence the persistence of pixels at the edge of the spot creating a higher than expect persistence in these pixels and therefore a seemingly premature rise of the persistence down to equivalent illuminations of about half full well. The spread of start of the transition zone seems entirely attributed to the surface trapping caused by diffusion of excess charge from neighboring saturated pixels, which is never present in flat fields. The undetected transition zone during the low flux illumination needs further investigations.

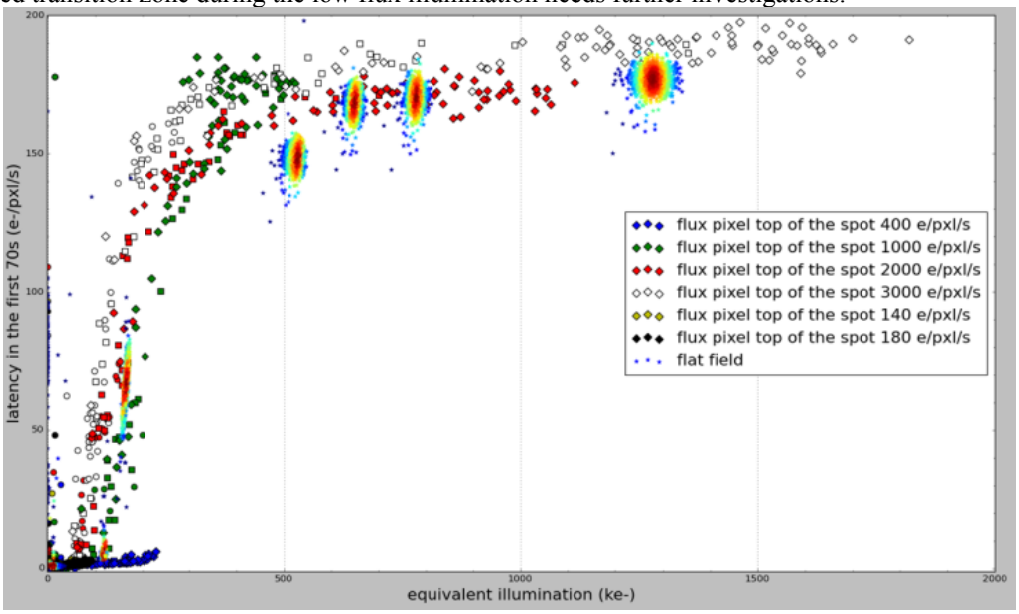

Figure 14: Persistence behavior in spot and flat field illumination with the equivalent illumination.

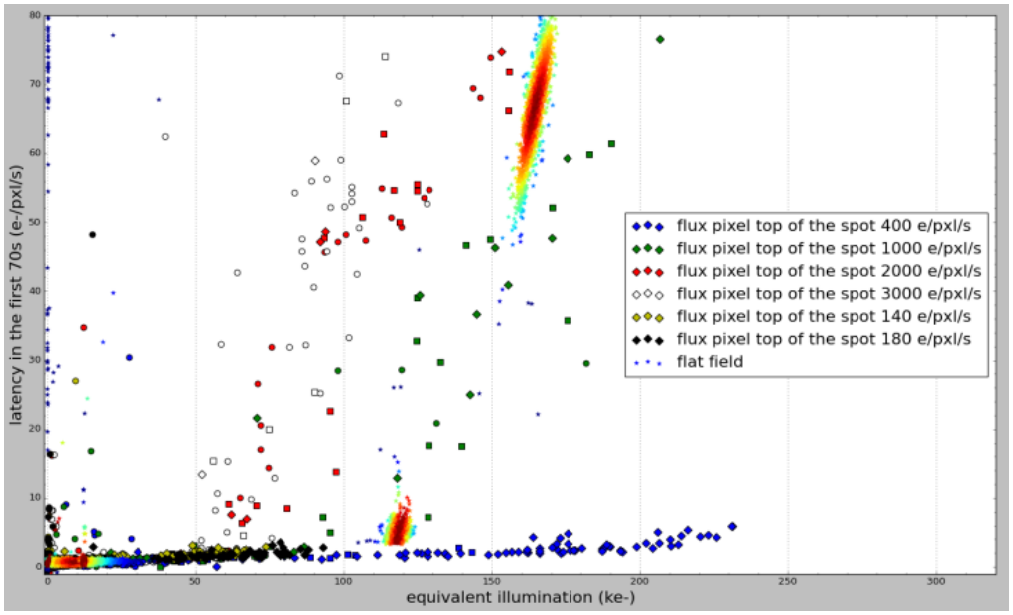

Figure 15: Persistence behavior zoom on the low equivalent illumination area

4. MEASUREMENT OF INTRA-PIXEL RESPONSE SHAPE

Using the spot projector system at focus and the 3-axis translation stage, the intra-pixel response shape of the HAWAII-2RG detector has been be measured.

4.1 Focus determination

For the 3 wavelengths (1100nm, 1550nm, 1950nm), the scan in the optical axis direction was performed to determine the best focus position. The spot was then fitted by a Gaussian in two dimensions and the position giving the smallest FWHM in the two directions was used to determine the optimum focus position. Figure 16 shows the evolution of the FWHM with the z optical axis at 1100nm. In this case, best focus is achieved at 48mm distance.

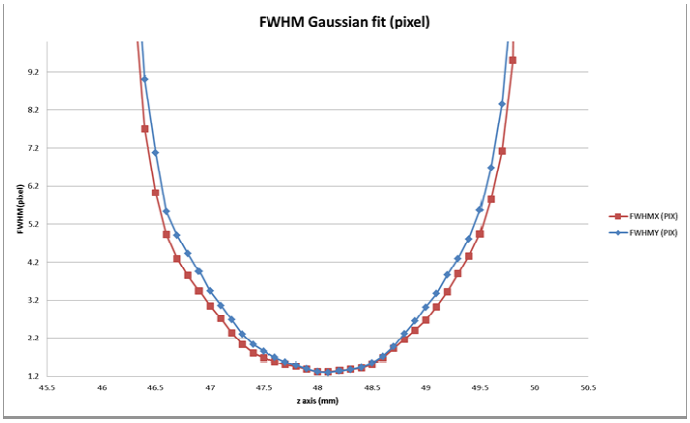

Figure 16: Evolution of the FWHM of the pixel for different position of the spot projector in the optical axis.

4.2 Scan through pixels

Once the focus position is found for each wavelength, the scan through a pixel can be performed.

The first scan was performed over a 3x3 pixel region, by moving the spot position in successive 2µm-steps. For each spot position a Correlated Double Sampling (CDS) readout was performed and the centroid of the imaged spot was then computed; this allowed to determine the spot position in a detector coordinate system (x and y axis). Figure 17 shows the centroids of the spot for a scan of a 3x3 pixels region at 1550nm.

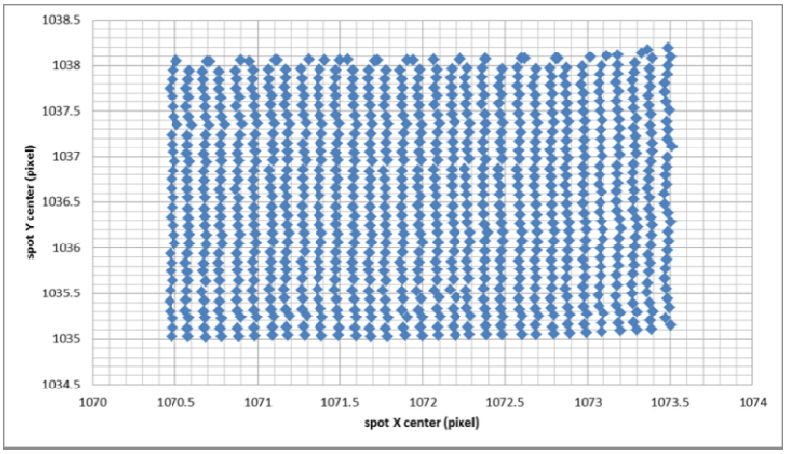

Figure 17: Centroid position for each spot position during a scan over 3 by 3 pixels at 1550nm.

4.3 Extraction of the pixel response

The signal received by one pixel can then be plotted with the spot position as shown in Figure 18. The single pixel response is symmetric in both directions. A signal is measured in the pixel when the spot is located on adjacent pixels due to lateral charge diffusion, capacitive coupling as well as the projected Airy disk.

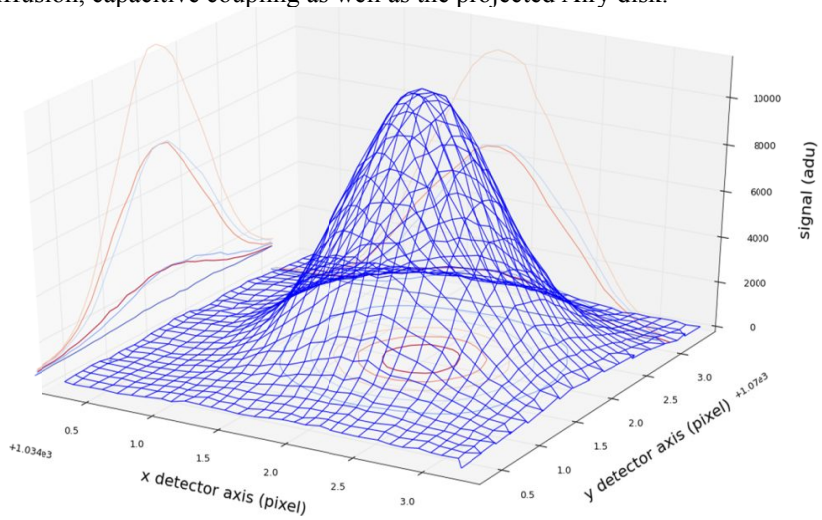

Figure 18:Two-dimensional response of a single pixel at 1100nm.

The pixel response of the array of scanned pixels at 1550nm are shown in Figure 19..

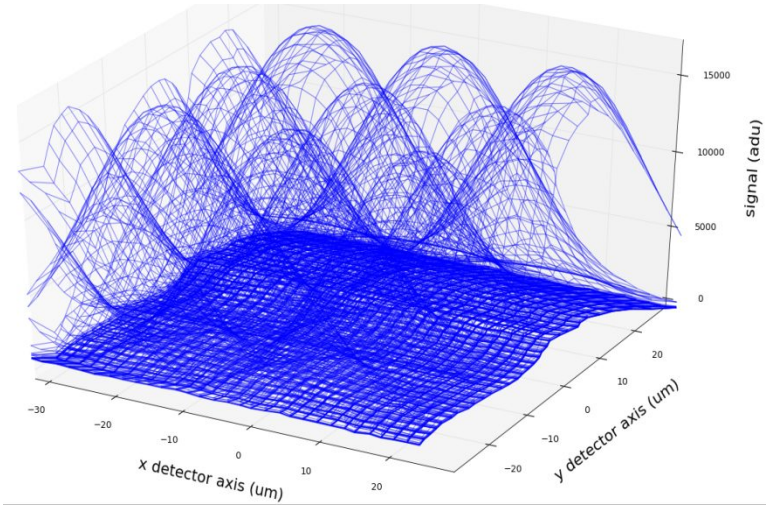

Figure 19: Two-dimensional response of a 4x4 pixels at 1550nm.

The true pixel response can be then derived. Instead of using a difficult 2D de-convolution of the data, a convolution using each component of the pixel response is used to fit the measured data. This method starts by convolving a boxcar representing the pixel with the Airy disk coming from the spot projector. The next step is to add lateral diffusion proportional to the hyperbolic secant and containing the diffusion length. The diffusion length, as a first approximation and used in previous intra-pixel measurement in [5] and [6] can be chosen to be identical to the detector cut-off of 2.3µm. The last step is to add the inter-pixel capacitance, which is known to be 0.6%. The main contributor in the quality of the fit is the diffusion length and the F-number of the projected Airy disk.

While the F-number was measured to be F#10 at 850nm, the best fit to the data is found to be F#13 at 1100nm. The best fit at the other wavelengths (1550nm, 1950nm) shows a best fit for F#13 as well (see Figure 20).

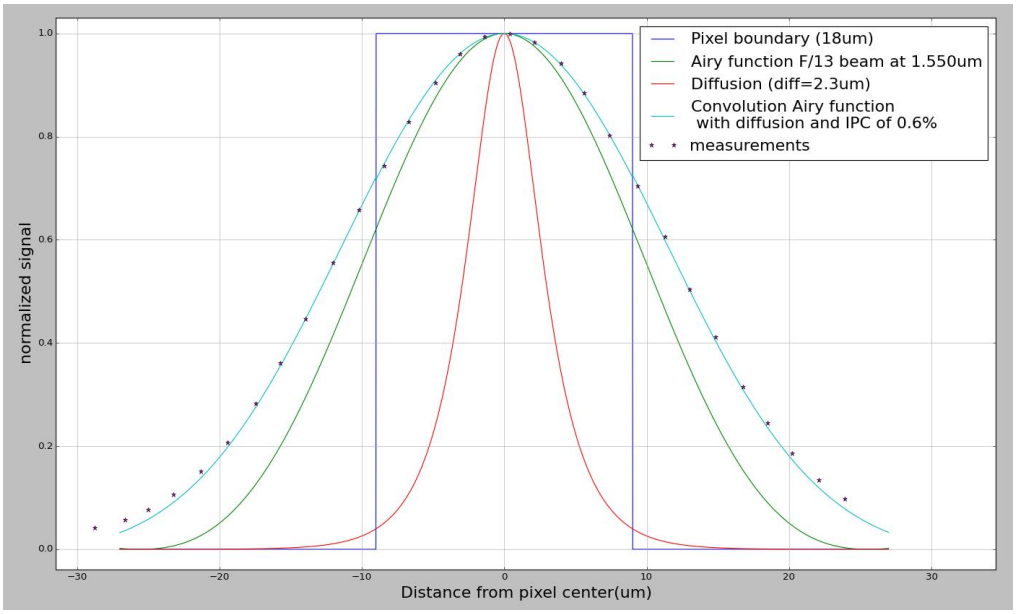

Figure 20: Fit of the intra-pixel response convolved with the Airy function at 1550nm

Once the best fit is obtained, the response of the pixel can be deduced by removing the impact of the Airy function (see Figure 21).

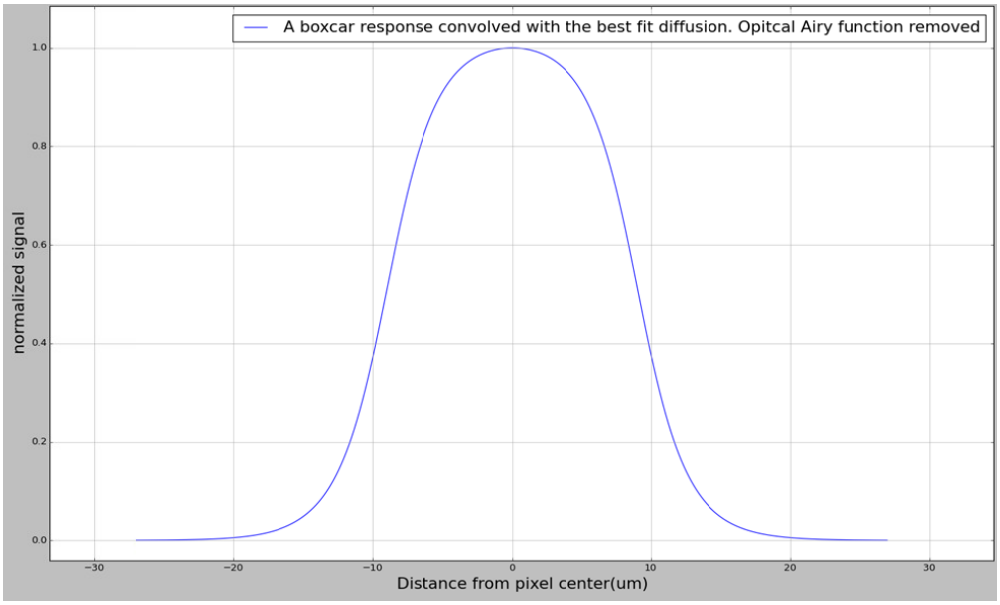

Figure 21: Pixel response function with the effects of the Airy function removed.

4.4 Photometric impact of intra-pixel variations

For each position of the spot inside a pixel, the signal received inside a given photometric window can be summed. The standard deviation of the sums computed for each position of the spot inside a pixel will give the photometric impact of the intra-pixel variation assuming the fitted F#13 beam.

To decrease the photon shot noise, 60 CDS were recorded for each spot position inside a pixel. For each position, the sum of the signal in a window of 7x7 pixels was recorded. This resulted in 51h of data acquisition, which was the limit set by the cryostat LN2 hold time. The ESTEC computing grid has been used to process the data in order to gain a factor 5 compared to a local machine . A more detailed data analysis is on-going, as the control of the lamp stability is essential to reach the needed measurement accuracy. The QTH lamp was initially monitored with a silicon sensor. Any variation on the near-infrared wavelength range could not be monitored. To improve the accuracy data on the HAWAII-2RG outside of the spot will be used to correct the lamp variations at the correct wavelength.

5. CONCLUSION

A Euclid pre-development SCS produced for the Euclid mission was successfully integrated in a test bench at ESTEC for two test campaigns, one to compare the persistence behavior in flat field and spot illumination, and the second to measure the photometric impact of the intra-pixel variations projecting a F#10 Euclid-like beam.
The persistence test using the spot showed that fluences above full well cause a lateral diffusion of the excess charge into adjacent pixels along the surface together with its corresponding surface trapping. The dark image after illumination then shows a much higher persistence signal in these adjacent pixels than expected from the recorded fluence under saturation. This effect does not appear in flat field illumination data due to the little signal contrast between pixels.
The persistence behaviour of one pixel depends not only on the flux it received, but as well on the soaking time in saturation of its neighbor pixels.
To quantify the photometric impact of the intra-pixel variation, a F#10 Euclid-like beam has been projected on the detector. The response of one pixel has been derived and fitted with a PSF simulation including diffusion and IPC effects. The stability and control of systematics are key parameters to the photometric impact. A detailed analysis is still on-going.

REFERENCES

[1] Laureijs, R.J., et al, “The Euclid Mission”, Proc. SPIE 7731, (2010)
[2] Verhoeve P. et al. , “ESA's CCD test bench for the Euclid visible channel”, Proc. SPIE 8453, (2012)
[3] Smith, R.M., et al., “A theory for image persistence in HgCdTe photodiodes”, Proc. SPIE 7021, (2008)
[4] Smith, R.M., et al., “Calibration of image persistence in HgCdTe photodiodes”, Proc. SPIE 7021 (2008)
[5] Long, K.S, et al., “Persistence in the WFC3 IR Detector”, The 2010 STScI Calibration Workshop Space Telescope Science Institute, (2010)
[6] Cheng, L., “Interpixel capacitive coupling,”, MS Thesis, Center for Imaging Science - Rochester Institute of Technology, (2009)
[7] Giardino,G., et al., “Noise properties and signal-dependent interpixel crosstalk of the detectors of the Near-Infrared Spectrograph of the James Webb Space Telescope”, Opt. Eng. Vol.52, Iss.3, (2013)
[8] Barron, N. et al., “Subpixel response measurement of near-infrared detectors,” PASP 119, 466–475, (2007)
[9] Hardy, T., et al., “Intra-pixel response of the new JWST infrared detector arrays”, Proc. SPIE 9154, (2014)